End Bearing Capacity of Tapered Piles in Sands using Cavity Expansion Theory

Manandhar, Suman
Post Doctoral Fellow, Department of Civil and Structural Engineering, Kyushu Univerisity

Yasufuku, Noriyuki
Professor, Department of Civil and Structural Engineering, Kyushu University

出版情報：九州大学工学紀要. 71 (4), pp.77-99, 2011-12. 九州大学大学院工学研究院
バージョン：
権利関係：

Memoirs of the Faculty of Engineering, Kyushu University, Vol. 71, No. 4, December 2011

End Bearing Capacity of Tapered Piles in Sands using Cavity Expansion Theory

by

Suman MANANDHAR* and Noriyuki YASUFUKU**

(Received November 5, 2011)

Abstract

The mechanism of tapered pile through small scale model tests has shown the increment of effective failure zone around the pile tip area with increasing tapering angle. On the load-settlement curve during pile penetration, evidences of model tests showed the increase in end bearing behavior by tapered piles. The analytical spherical cavity expansion theory has been utilized to evaluate the end bearing capacity. In the proposed model, the effect of angle of tapering has been introduced to compute the end bearing capacity of tapered piles. The test results and proposed model show that the tapering angle affects the end bearing resistance comparing with conventional straight piles on different types of sands at different relative densities. The studies incorporating model tests, prototype tests and real type pile tests have been validated and predicted well the proposed model.

Keywords: End bearing capacity, Spherical cavity expansion theory, Tapered piles, Relative density, Sands

1. Introduction

The pile end bearing capacity in cohesionless soils depends on the compressibility of soil, shear stiffness and strength. In addition, the end bearing capacity is also affected by the angle of tapering which is a function of angle of internal friction [1)]. However, except by few researchers, there was no significant research relating to influence of tapering on the end bearing mechanism. Thus the influence of tapering effects has been noted with spherical cavity expansion theory on model tests, proto type and real pile tests respectively. Not only the radial stress and skin friction have been well affected through tapered pile, the end bearing mechanism has also been influenced when penetrated downward in a frictional mode. When the shape of the pile is altered into tapered type from its straight-sided cylindrical shape, it can easily be noticed that the weight and volume of the pile surcharges directly down to the ground and mechanism has been changed when driving into the ground. Therefore, it is most important to consider the tapering effects of pile during evaluating end bearing capacity of tapered piles [2)]. There are two main methods to evaluate the end bearing capacity, a semi-empirical method using SPT-N values and a theoretical approach based on the geomechanical considerations. In theoretical methods of geomechanics, the cavity expansion theory is very popular within geotech connoisseur [3-5)]. Yasufuku et al. (1995, 2001) has successfully

*Post Doctoral Fellow, Department of Civil and Structural Engineering
** Professor, Department of Civil and Structural Engineering

derived the evaluation technique for the end bearing capacity in non-displacement straight cylindrical piles using spherical cavity expansion theory for closed solution [6-7]. In this paper, the spherical cavity expansion theory has been asserted to evaluate the end bearing capacity of tapered piles based on axial cylindrical model tests.

2. Visual interpretation of end bearing mechanism

The failure zone is developed along soil-pile interface with partly upheaving laterally and disturbs the soil below the pile tip, when pile is penetrated in a downward frictional mode. Partly consolidation develops around soil-pile interface when soil compresses elastically below the critical depth. Medium dense sand reveals dragging of thin layer of soil particles and compresses laterally such that the displacements had decreased according to parabolic law with increasing the diameter of the disturbed zone around the pile approximately six times the diameter of the pile [8]. Besides, the failure zone exceeds below the tip of the pile when angle of tapering has changed. Hence, it is imperative to understand the mobilized mechanism pile tip when different tapered piles are penetrated. In order to comprehend the effect of tapering, small model chamber pile load tests were carried out with different types of piles in dense ground.

Three steel chromium piles, having same length and same pile tip diameter have chosen for pile loading test (**Table 1**). The fully equipped pile load cylindrical chamber has dimensions of 460 mm height and 280 mm diameter facilitated with the advantage of easy split up of the chamber into two halves to observe the end bearing mechanism of piles. Toyoura (TO) sand was used at 80 % relative density by free fall methodology. Here, TO sand was partitioned into black-colored and non-colored soil. One centimeter black-colored soil was filled at the same relative density followed by non-colored TO soil. Piles were installed at the center of the chamber as cast-in-place type. Then layered modeled ground was prepared up to depth of 400 mm and covered by upper plate in order to give the overburden pressure during the test. Then pile was jacked with load cell, dial gauge connected with data logger and speed control box (**Fig. 1a**). Then, pile had been mobilized at speed of 4 mm/min up to 100 mm for each test.

After loading, the chamber was immersed in the water bath to prevent from failure when chamber would be split into two halves. After removing from the water bath the chamber had been split up to two halves and trimmed carefully (**Fig. 1b**). **Figure 2** shows the end bearing mechanism of three different piles in which visual measurements have been carried out.

The visual inspection and measurements of dimensions of disturbed soil particle zone below the pile tip have been termed as effective length. After the pile penetration, effective length of the disturbed soil has been measured from the tip of the pile visually to the point of maximum curvature below the tip of the pile and plotted for all piles as shown by **Fig. 3**. The failure mode at the pile tip settlement had seemed to be increased relatively in tapered piles. This increment of failure zone with increase in tapering angle at the toe appends the tapering effects of the pile in soils during penetration towards the depth.

3. Substantiation of model tests

3.1 Sample preparation and test procedures

Two different model grounds were prepared at relative densities of 60 % and 80 % respectively (**Table 2**). The chromium plated three steel model piles, one straight (S) and two taper-shaped (T-1 and T-2), with equal lengths and same tip diameters were used for pile penetration (**Table 1**) which have load cell at the tip to measure load connected by cord.

Figure 4 (a) represents the pile load cylindrical chamber which is 1000 mm in height and 750 mm diameter. It is well connected with air cylinder, displacement gauge, loading jack and loading cell. Upper plate transfers overburden pressure to the model ground vertically.

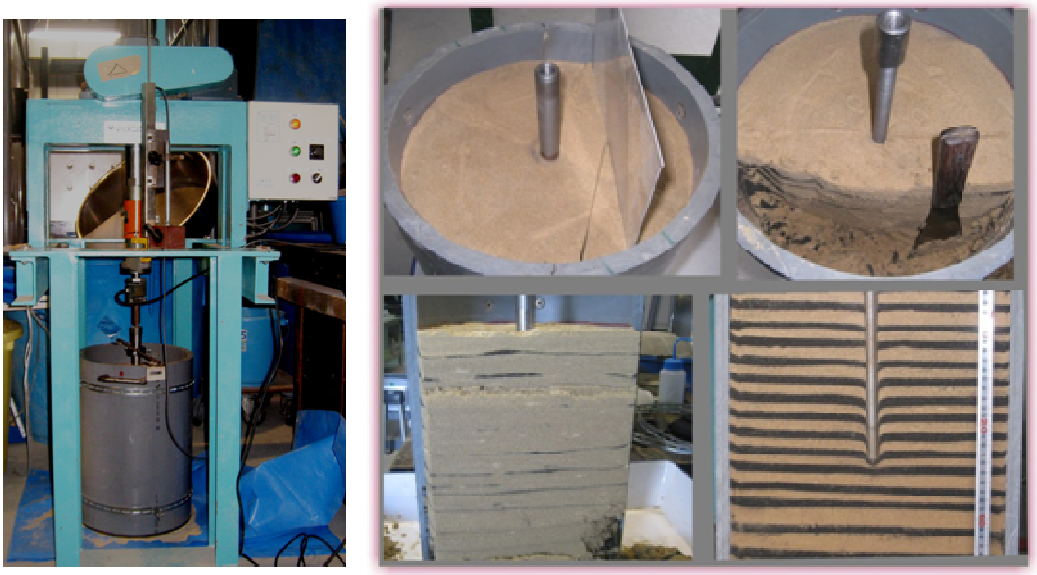

Fig. 1 Systematic process of pile loading; **(a)** Small pile load test apparatus for the mobilized mechanism (figure is not in scale) and **(b)** Steps to visualize the mobilized mechanism after pile load testing.

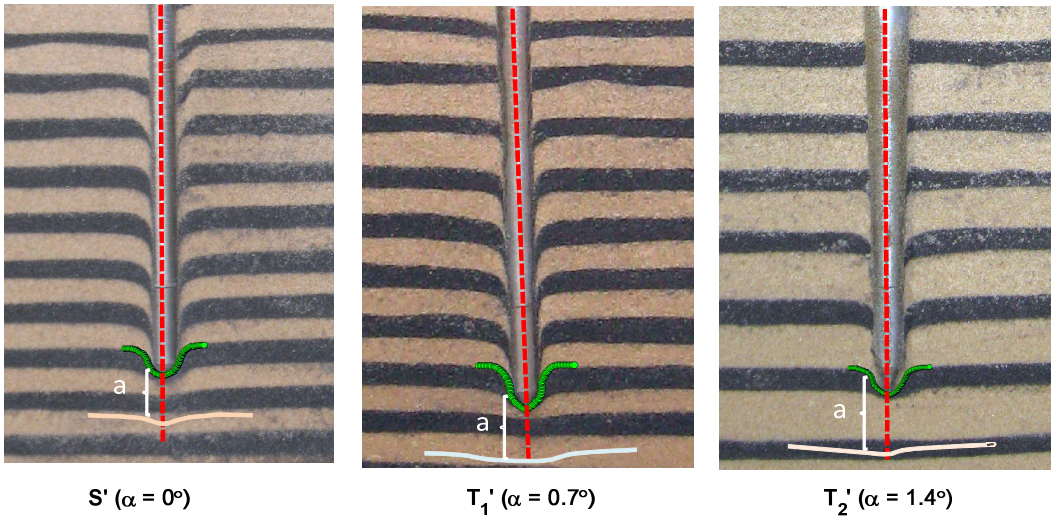

Fig. 2 Mobilized mechanism of pile: a = effective length at the pile tip settlement.

Japanese Industrial System (JIS A 1224) and Japanese Geotechnical Standards (JGS 0161) [9] have been used to determine the maximum and minimum dry densities of both sands and relative densities have been calculated (**Table 2**). A sample preparation method using multiple sieving was used which can give a wide range of specimen density by height of fall and nozzle diameter [10]. Different nozzle area and/or diameter significantly change the densification of the ground. In this case, height of falling was determined to make the required ground keeping constant nozzle area.

K-7 sand was fallen freely from the height of 1400 mm and spread uniformly on the chamber by rotating homogenously while TO sand was fallen from 700 mm height to meet the required density. Height was controlled by lifting the multiple sieve apparatus. The pile was installed at the height where soil meets at the level of 710 mm from the bottom. Further, soil was poured up to 930

mm as shown by **Fig. 4 (b)**. Then upper part was carefully closed by plate and load cells at pile head and tip were connected. Finally, pneumatic air pressure of 50 kPa was set up to furnish the overburden pressure (σ_v) vertically through upper plate and pile was penetrated down up to 200 mm as installation of pile at the rate of 5 mm/min to facilitate in cast-in-place pile condition. Minimum fifteen hours time is required to relief the stress during installation. Afterwards, pile loading was carried out up to 0.4 settlement ratio.

Table 1 Geometrical configuration of different types of piles.

Types of Model Piles	Naming	L mm	D_t mm	d mm	α °	FRP reinforcement direction	Modulus of elasticity (GPa)
Smallest model steel piles	S′	345	13	13	0.00	na	$2X10^9$
	T_1'	345	20	13	0.70	na	$2X10^9$
	T_2'	345	28	13	1.40	na	$2X10^9$
Smaller model steel piles	S	500	25	25	0.00	na	$2X10^9$
	T-1	500	35	25	0.70	na	$2X10^9$
	T-2	500	45	25	1.40	na	$2X10^9$
Prototype FRP piles	FC	1524	168.3	168.3	0.00	na	31.86
	T-3	1524	170.0	198.0	0.53	0°	33.20
	T-4	1524	159.0	197.0	0.71	0°	33.15
	T-5	1524	155.0	215.0	1.13	0°	33.15

Note: L: length of pile; D_t: diameter at the pile head; d: pile tip diameter; FRP: fiber-reinforced polymer; α: angle of tapering; na: not applicable;

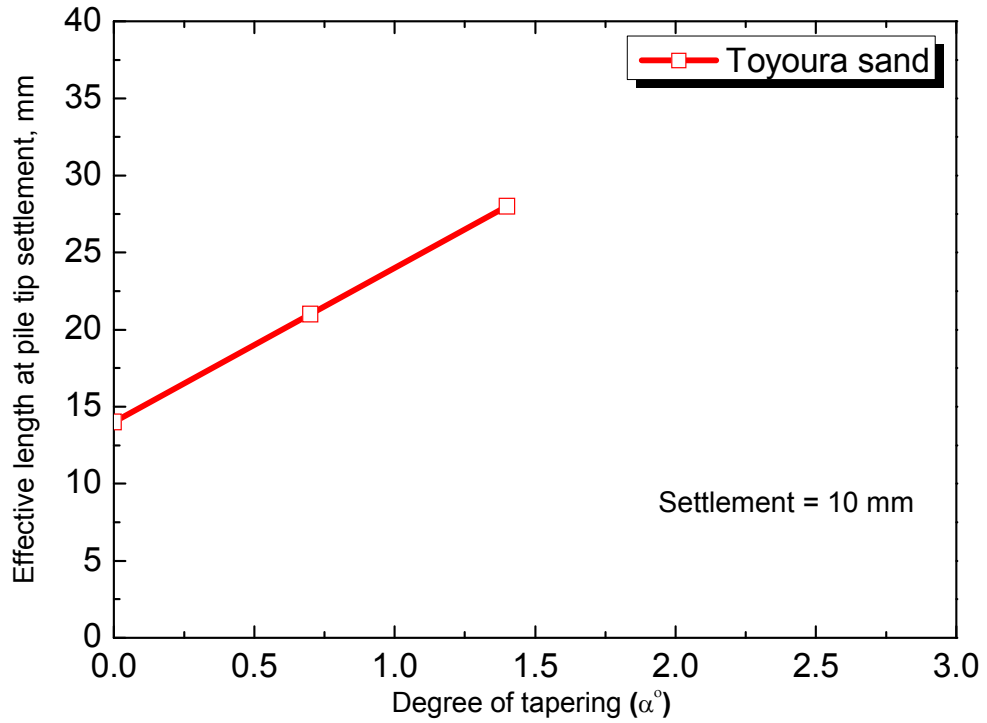

Fig. 3 Visually measured pile tip failure zone.

Table 2 Geotechnical parameters of different types of soil.

Descriptions		TO	K-7	Fanshawe brick sand (Sakr et al.) [11-13]
Density of particles, (g/cm^3)	ρ_s	2.65	2.62	2.68
Maximum density, (g/cm^3)	ρ_{max}	1.64	1.60	1.772
Minimum density, (g/cm^3)	ρ_{min}	1.34	1.19	1.466
Density at I_D 80 %, (g/cm^3)	ρ_{80}	1.58	1.52	na
Density at I_D 60 %, (g/cm^3)	ρ_{60}	1.52	1.43	na
Maximum void ratio,	e_{max}	0.98	1.20	0.794
Minimum void ratio,	e_{min}	0.62	0.64	0.484
Void ratio at I_D 90 %,	e_{80}	na	na	0.68
Void ratio at I_D 80 %,	e_{80}	0.68	0.73	na
Void ratio at I_D 60 %,	e_{60}	0.74	0.83	na
Effective grain size, (mm)	D_{10}	na	na	0.14
Mean grain size, (mm)	D_{50}	na	na	0.26
Uniformity coefficient,	U_c	1.40	4.0	2.143
Coefficient of curvature,	U'_c	0.86	1.21	0.905
Percent fines, (%)	F_c	1.10	14	na
Peak stress, (deg) º	ϕ	42.00	47.00	37.00
Critical stress state, (deg) º	ϕ'_{cv}	32.00	34.00	31.00

3.2 Test results

The model pile load test can measure load at the pile tip and at the head directly during the test. Besides, it has merits over computing skin friction around the shaft of the pile by taking differences between loads at pile tip and head in kN. Since, this paper is mainly focused on end bearing capacity of piles, the skin friction and total bearing capacity have been ignored so far.

Figure 5 represents load governed by pile tip of straight and taper-shaped piles of K-7 sand and TO sand. With increasing the tapering angle the load were gradually increased in a considerable amount at high normalized settlement ratio. Here, S is considered as settlement and D is the pile tip diameter. Further, the normalized total end bearing capacity has been plotted by dividing mean effective stress σ' which is the mean of radial and vertical stresses (i.e. $\sigma' = (\sigma_0 + \sigma_v)/2$). At rest, for normally consolidated soil the radial stress can be obtained by putting 0.5 value in the relation between radial and overburden stresses (i.e. $\sigma_0 = K_0\, \sigma'_v$); where K_0 is the coefficient of earth pressure at rest which are strictly related to dry unit weight of the ground and depth. Both sands trace the higher capacities with increasing tapering angles.

Figure 6 explains the normalized total end bearing capacity of both sands which clearly show the tapering effects with increasing tapering angle in different relative densities. These evidences from small model tests clearly show the benefits of tapered piles on end bearing capacity. Based on it, the evaluation method will be proposed and validate its liability verifying with prototype and real pile references in the next section.

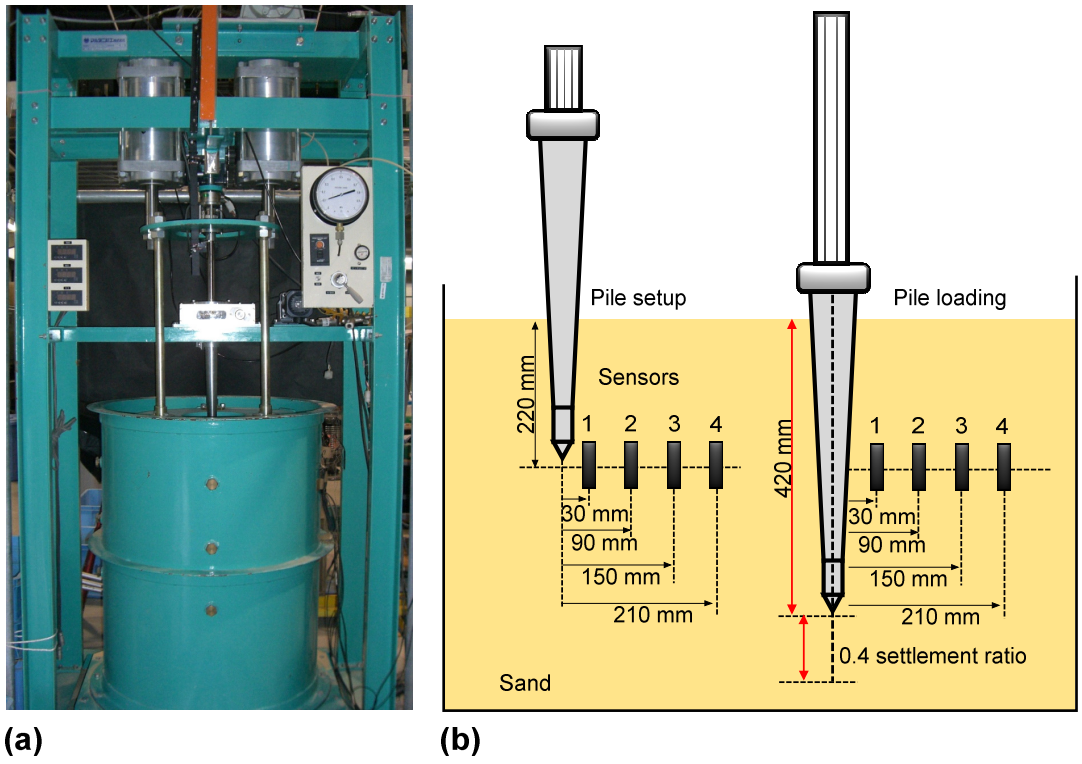

Fig.4 Systematic process of pile loading test; **(a)** Pile load apparatus and **(b)** Cast-in-place pile set up and pile loading (figure is not in scale).

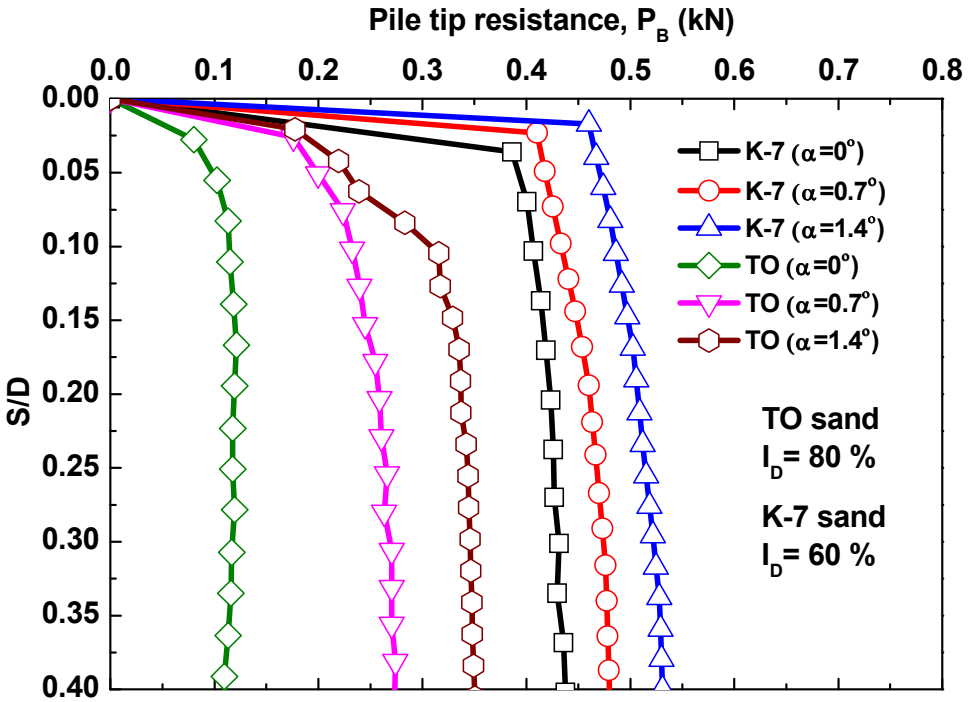

Fig. 5 Pile tip resistance on K-7 sand and TO sand.

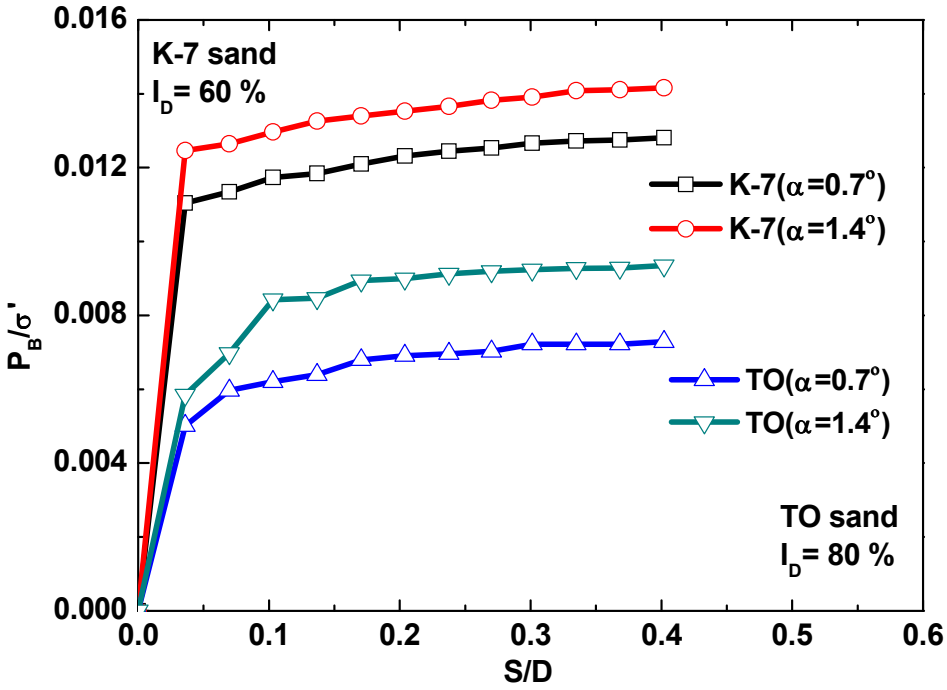

Fig. 6 Normalized total end bearing capacity of K-7 sand and TO sand.

4. Evaluation of end bearing capacity using cavity expansion theory

The pile end bearing capacity in cohesionless soils depend on the compressibility of soil, shear stiffness and strength. Compressibility diverges broadly for different types of soils governing through incompressible silica sands to highly compressible carbonate sands. The analytical solution using spherical cavity expansion theory to evaluate the end bearing capacity of cylindrical pile in closed form has been established by Yasufuku et al (1995, 2001). Based on this evaluation technique, the model has been improved to evaluate the end bearing capacity of tapered piles. **Figure 7** gives the modified failure mechanism which was initially postulated by Yasufuku et al.[6-7] for frictional soils with cavity expansion pressure p_u proposed by Vesic`[2] to compute the ultimate bearing capacity q_{pcal}. In the context of end bearing capacity of tapered piles, it is assumed that the use of cavity expansion theory is a rigid cone of soil exists beneath the pile tip with the angle ψ, ($= \pi/4 + \phi'/2+\alpha$) and outside the conical region, the zone is subjected to isotropic stress which is equal to the cavity expansion pressure p_u. Furthermore, active earth pressure conditions σ_A *[*$= q_{pcal}$ *{(1 -* $\sin(\phi'_{cv} + 2\alpha)$*)/ (1 +* $\sin(\phi'_{cv} + 2\alpha)$*)}]* are considered to exist immediately beneath the pile tip along AC plane. Then the moment is considered at point B as shown by **Fig. 7** for the cavity expansion pressure p_u, ultimate end-bearing pressure q_{pcal} and the active earth pressure σ_A. The ultimate bearing capacity q_{pcal} can be expressed as follows. The detail derivation is shown in Appendix I.

$$q_{pcal} = \frac{1}{1-\sin\left(\phi'_{cv}+2\alpha\right)} p_u \qquad (1)$$

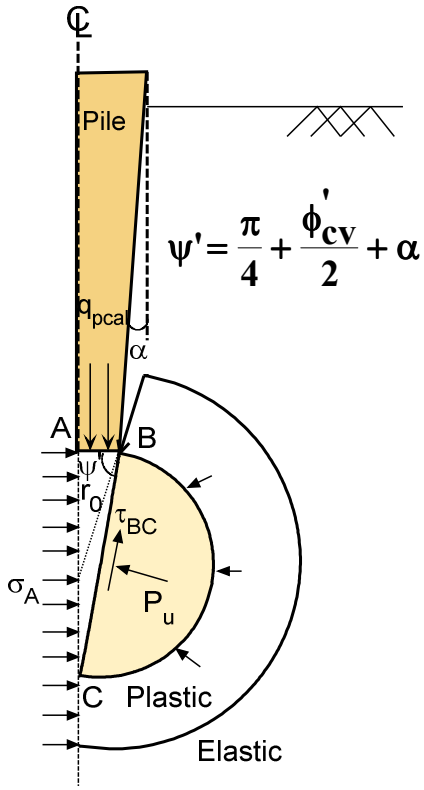

Fig. 7 Failure mechanism of tapered pile in cavity expansion solution.

Based on Vesic` theory [3], the cavity expansion pressure p_u is given by:

$$p_u = F_q \frac{(1+2K_0)}{3}\sigma_v' \tag{2a}$$

$$F_q = \frac{3\left(1+sin\phi_{cv}'\right)}{\left(3-sin\phi_{cv}'\right)}[I_{rr}]^{\left(4sin\phi_{cv}'\right)/3\left(1+sin\phi_{cv}'\right)} \tag{2b}$$

$$I_{rr} = \frac{I_r}{1+I_r\Delta_{av}} \tag{2c}$$

$$I_r = \frac{3G}{(1+2K_0)\sigma_v' tan\phi_{cv}'} \tag{2d}$$

Where F_q, I_{rr}, and I_r are called dimensionless spherical cavity expansion factor, reduced rigidity index and rigidity index respectively. These parameters are related to friction angle ϕ', shear stiffness G and average volumetric strain Δ_{av} for the plastic zone around a cavity, together with the coefficient of earth pressure at rest K_0 and overburden pressure σ_v'. I_r gives a ratio of shear stiffness to strength and I_{rr} is considered to be a parameter representing the soil compressibility, in which shear stiffness, shear strength and average volumetric strain are combined.

σ_v' is basically computed as an averaged unit weight γ_{av} ($=\gamma_{av}z$). Based on theoretical relation to plastic equilibrium, K_0 and ϕ_μ' is the angle of interparticle sliding friction, proposed by Ochiai (1976) [14] for normally consolidated sands, together with a relationship between critical state friction angle ϕ_{cv}' and ϕ_μ' as below:

$$K_0 = \frac{1-sin\phi_\mu'}{1+sin\phi_\mu'} \tag{3}$$

$$sin\phi_{cv}^{'} = \frac{2sin\phi_{\mu}^{'}}{1+sin\phi_{\mu}^{'}} \tag{4}$$

Combining Eq. (3) and Eq. (4), the K_0 value can be expressed as a function of $\phi_{cv}^{'}$ as follows:

$$K_0 = 1 - sin\phi_{cv}^{'} \tag{5}$$

Affirming the critical state friction angle $\phi_{cv}^{'}$ is effective and rational as a strength parameter in practical applications [15-18], the friction angle guarantees the minimum shear strength under the same initial condition and it is also considered to be independent of soil density, initial fabric and confining pressure. The value of $\phi_{cv}^{'}$ of sands is almost equal to the maximum friction angle under the high confining stress, which will be mobilized below the pile tip [19-20]. Therefore, the $\phi_{cv}^{'}$ is recommended for estimating the pile end-bearing capacity of sands and Eq. (1) can be written as:

$$q_{pcal} = \frac{3\left(1+sin\phi_{cv}^{'}\right)}{\left(1-sin\left(\phi_{cv}^{'}+2\alpha\right)\right)\left(3-sin\phi_{cv}^{'}\right)}[I_{rr}]^{\left(4sin\phi_{cv}^{'}\right)/3\left(1+sin\phi_{cv}^{'}\right)} \times \left(\frac{1+2K_0}{3}\right)\sigma_v^{'} \tag{6}$$

The value of K_0 is computed from Eq. (5) and I_{rr} is evaluated from Eq. (2c). To determine the q_{pcal} value with parameter I_{rr}, the evaluation of G and Δ_{av} are required to know.

Based on theoretical approach, Yamaguchi (1975) [20] expressed the maximum shear strain as:

$$\gamma_{max} = \frac{3p_0 sin\phi_{cv}^{'}}{\left(3-sin\phi_{cv}^{'}\right)G}\left(\frac{b}{r}\right)^3 \approx \frac{3p_0 sin\phi_{cv}^{'}}{4G}\left(\frac{b}{r}\right)^3 \tag{7}$$

Where, p_0, b, and r are ground stress around the pile tip, radius of plastic and radius distance from cavity center. The maximum shear strain computed from this equation corresponds to the shear stiffness used in the cavity expansion analysis was more or less in the order of 10^{-3}. An empirical equation to predict the G value in the strain level of 10^{-3} from the measured N-value [21] as:

$$G = 7.0N^{0.72}\ (MPa) \tag{8}$$

The penetration resistance is assumed to increase with the square of the relative density and directly proportional to the effective overburden pressure and inversely proportional to the void ratios [22].

$$N = \frac{9I_D^2}{(e_{max}-e_{min})^{1.7}}\left\{\frac{\sigma_v^{'}}{98}\right\}^{0.5} \tag{9}$$

Where, I_D is relative density and e_{max} and e_{min} are maximum and minimum void ratios. Now, substituting values of N from Eq. (9) to Eq. (8), the empirical correlation between G-value and I_D can be expressed as:

$$G = 7.0\left\{\frac{9I_D^2}{(e_{max}-e_{min})^{1.7}}\left\{\frac{\sigma_v^{'}}{98}\right\}^{0.5}\right\}^{0.72} \tag{10}$$

In accordance with Vesic` [3], the determination of Δ_{av} requires two or three isotropic and triaxial compression tests to reflect the soil compressibility due to compression and shear which is difficult to use in practical application. Thus, Yasufuku et al.[6] suggested the following empirical equation to compute the Δ_{av} value as a function of I_r in a simple manner.

$$\Delta_{av} = 50(I_r)^{-1.8} \tag{11}$$

Substituting Eq. (2d) into Eq. (11), Eq. (11) is rewritten as a function of G, K_0, $\sigma_v^{'}$, and $\phi_{cv}^{'}$ as follows:

$$\Delta_{av}= 50\left\{\frac{\left(\frac{1+2K_0}{3}\right)\sigma_v^{'}tan\phi_{cv}^{'}}{G}\right\}^{1.8} \tag{12}$$

This equation indicates the average volumetric stain Δ_{av} for a plastic zone around a cavity increases with increasing overburden pressure in the associated ground. Additionally, rearranging Eq. (12) and Eq. (6), the following equation can be expressed to estimate the ultimate pile end-bearing capacity.

$$q_{pcal} = \frac{A^{'}}{1-sin\left(\phi_{cv}^{'}+2\alpha\right)}\left\{\frac{\frac{G}{\sigma_v^{'}}}{B^{'}+D^{'}\left(\frac{G}{\sigma_v^{'}}\right)^{-0.8}}\right\}^{C'}\sigma_v^{'} \tag{13a}$$

Where,

$$A^{'} = \frac{3\left(1+sin\phi_{cv}^{'}\right)}{\left(3-sin\phi_{cv}^{'}\right)}\left(\frac{1+2K_0}{3}\right) \tag{13b}$$

$$B^{'} = \left(\frac{1+2K_0}{3}\right)tan\phi_{cv}^{'} \tag{13c}$$

$$C^{'} = \frac{4sin\phi_{cv}^{'}}{3\left(1+sin\phi_{cv}^{'}\right)} \tag{13d}$$

$$D^{'} = 50\left\{\left(\frac{1+2K_0}{3}\right)tan\phi_{cv}^{'}\right\}^{1.8} \tag{13e}$$

The Kondner type of hyperbolic curves are useful for predicting the load settlement curves of non-displacement piles in virgin loading [23-25]. Thus, a simple hyperbolic function is assumed to be applicable for estimating the relationship between the applied pile tip stress, q_{cal}, and the corresponding normalized pile tip settlement, S/D as:

$$q_{cal} = \frac{\frac{S}{D}}{n+m\left(\frac{S}{D}\right)} \tag{14}$$

Where n and m are experimental parameter correspond to the inverse values of suitable initial shear stiffness and an ultimate pile stress respectively. Moreover, when introducing reference displacement $(S/D)_{ref}$ presented by Hirayama [25] which is empirically derived based on many reliable loading test data for non-displacement piles in sands, expressed as the normalized settlement S/D required to mobilize the half of the ultimate end bearing capacity q_{pcal}, the inverse of the initial shear stiffness is articulated such that:

$$n = \frac{\left(\frac{S}{D}\right)_{ref}}{q_{pcal}} \tag{15a}$$

$$\left(\frac{S}{D}\right)_{ref} = 0.25 \tag{15b}$$

Rearranging Eq. (15) into Eq. (14), it can be expressed as follows:

$$q_{cal} = \frac{\frac{S}{D}}{\frac{\left(\frac{S}{D}\right)_{ref}}{q_{pcal}}+\frac{\left(\frac{S}{D}\right)}{q_{pcal}}} = \frac{\frac{S}{D}}{\left\{0.25+\frac{S}{D}\right\}}q_{pcal} \tag{16}$$

4.1 Results and verification of the model

Small model and prototype pile materials have been considered to check the end bearing capacity using the proposed model. Properties of Toyoura (TO) sand, K-7 sand and Fanshawe brick sand have been used for evaluating the model. The parameters of TO sand K-7 sand and pile materials have been taken from S. Manandhar [1-2]. Similarly, Fanshawe brick sand and pile materials have been adapted from Sakr et al. [11-13]. The cylindrical fiber-reinforced polymer (FRP) FC pile and another three tapered FRP composite tapered piles have been considered for analyses. In brief, FRP, FC, is an off-the-shelf pipe with an average diameter of 162.4 mm and a ply angle of 55°. The FRP tapered piles were fabricated using glass filament wound (GFW). Six layers of GFW were placed at ply angles 0° (parallel to pile axis) and 90° (hoop layer) [11] (**Tables 1** and **2**).

The pile installation of Fanshawe brick sand has confined to low and high pressures respectively. Low pressure of initial radial stress 30 kPa and vertical pressure of 60 kPa as well as high pressure of initial radial stress 60 kPa and vertical pressure of 120 kPa have been performed at different depths and mobilized up to 0.4 normalized settlement ratios. The vertical pressure can be obtained by using simple formula which has been discussed in the previous section.

In the closed form cavity expansion theory, the total end bearing capacity is increased with increasing the tapering angles as shown in **Fig. 8** for both K-7 sand and TO sand. Higher density ground reflects the higher total end bearing capacity. When different radial stresses are furnished at the same density ground, high radial stresses govern the higher end bearing capacity in Fanshawe brick sand as shown by **Fig. 9**.

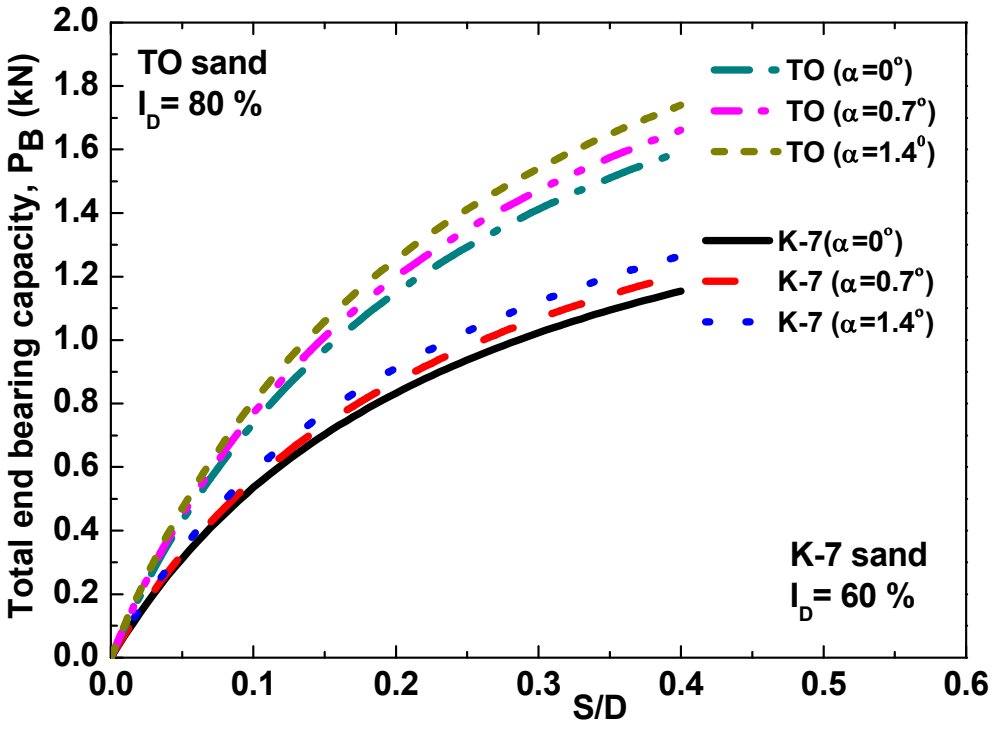

Fig. 8 Total end bearing capacity of TO and K-7 sands of different piles at normalized settlement ratio.

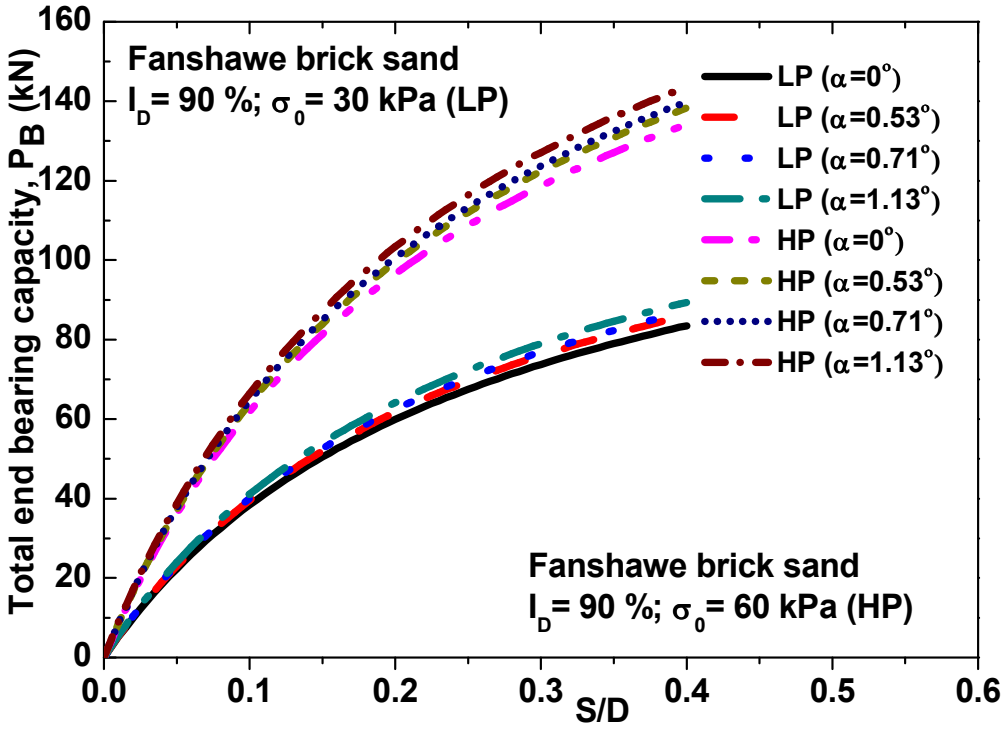

Fig. 9 Total end bearing capacity of Fanshawe brick sand of different piles at normalized settlement ratio.

Further, the total end bearing capacity measured in kN is calculated as:

$$P_B = q_{cal}\,\pi {r_b}^2 \tag{17}$$

Where, r_b is the radius of the pile tip at the middle point of the embedded pile section.

Substituting value of q_{cal} using Eqs. (1), (2), (13) and (16) into Eq. (17), the following arrangement can be obtained:

$$P_B = \frac{\frac{S}{D}}{\left\{0.25+\frac{S}{D}\right\}}\frac{1}{1-sin\left(\phi_{cv}^{'}+2\alpha\right)}A^{'}\left\{\frac{\frac{G}{\sigma_v^{'}}}{B^{'}+D^{'}\left(\frac{G}{\sigma_v^{'}}\right)^{-0.8}}\right\}^{C'}\sigma_v^{'}\,\pi {r_b}^2 \tag{18}$$

And assume that $(P_B)_{\alpha=0}$ is the total end bearing capacity of straight pile. When total end bearing capacity of tapered pile is normalized by dividing total end bearing capacity of straight pile, the following relation can be written in the form:

$$\frac{P_B}{(P_B)_{\alpha=0}} = \frac{\frac{\frac{S}{D}}{\left\{0.25+\frac{S}{D}\right\}}\frac{1}{1-sin\left(\phi_{cv}^{'}+2\alpha\right)}A^{'}\left\{\frac{\frac{G}{\sigma_v^{'}}}{B^{'}+D^{'}\left(\frac{G}{\sigma_v^{'}}\right)^{-0.8}}\right\}^{C'}\sigma_v^{'}\,\pi {r_b}^2}{\frac{\frac{S}{D}}{\left\{0.25+\frac{S}{D}\right\}}\frac{1}{1-sin\,\phi_{cv}^{'}}A^{'}\left\{\frac{\frac{G}{\sigma_v^{'}}}{B^{'}+D^{'}\left(\frac{G}{\sigma_v^{'}}\right)^{-0.8}}\right\}^{C'}\sigma_v^{'}\,\pi {r_b}^2} \tag{19}$$

Hence, the final relationship can be obtained as:

$$\frac{P_B}{(P_B)_{\alpha=0}} = \frac{\frac{1}{1-sin\left(\phi_{cv}^{'}+2\alpha\right)}}{\frac{1}{1-sin\,\phi_{cv}^{'}}} \tag{20}$$

This equation shows the relationship between angle of internal friction at critical state and tapering angle as the interdependent function which controls the total end bearing capacity of tapered piles. This verifies that, end bearing capacity depends on angle of internal friction at critical state condition and tapering angle of piles. When there is change in angle of tapering, the end bearing capacity will change along with given angle of internal friction independent of overburden pressure, confining pressure and shear modulus of soil. Hence, obtainable normalized ratios of total end bearing capacity for different sands have been plotted to verify this mechanism as shown by in **Figs. 10**, **11**, and **12** respectively. They show clear increment of total end bearing capacity with increasing degree of tapering at 0.1 settlement ratios for all types of soils and pile materials.

As the angle of tapering is the key factor to control the end bearing capacity, different tapering angles have been inserted to understand the pile behavior in sands. Model tests, prototype test described by Sakr et al. [11-13] and El Naggar et al. [26] and real type Rybnikov [27] pile have been used for study. Rybnikov [27] carried out tests in the Irtysh Pavlodar region of the former Soviet Union and used bored-cast-in-place tapered piles. The holes for the piles were drilled with endless screws. Seven different types of piles were accomplished having each length of 4.5 m, comprising five tapered piles and two cylindrical piles to understand the behavior of tapered piles clearly with respect to straight piles. In this study only geometry of pile materials have been considered for the analyses with assumption of soil properties governed by TO sand as shown by **Table 2**.

Figure 13 shows the effect of tapering angle in four types of soil and pile materials by taking the ratios of total end bearing capacity of tapered to straight piles for all soils. The result shows that about 10 % increase on the end bearing capacity for maximum tapered angle. It seems that the end bearing capacity is affected by angle of tapering and angle of internal friction only.

Proceeding, the measured and calculated results of end bearing capacity were taken to verify the model. The verification of the model has been accounted with adding various researchers' reference data to validate the model accurately. The measured and predicted results of end bearing capacity, measured in kPa, have been tabulated in **Tables 3** and **4** respectively. **Figure 14** shows remarkably fit with proposed model on evaluating end bearing capacity when many reference researchers' data have been utilized along with model tests. Different types of pile geometry with different types of sandy soils have been plotted in 1:1 ratio and shows that the accuracy of proposed model fits with the parameters used.

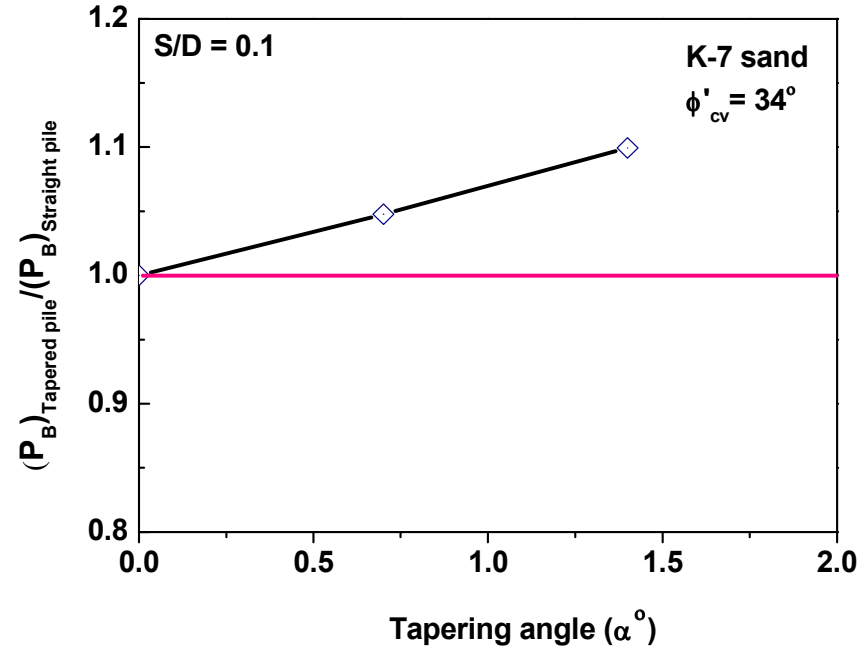

Fig. 10 Normalized end bearing capacity of K-7 sand at different pile tapering angle.

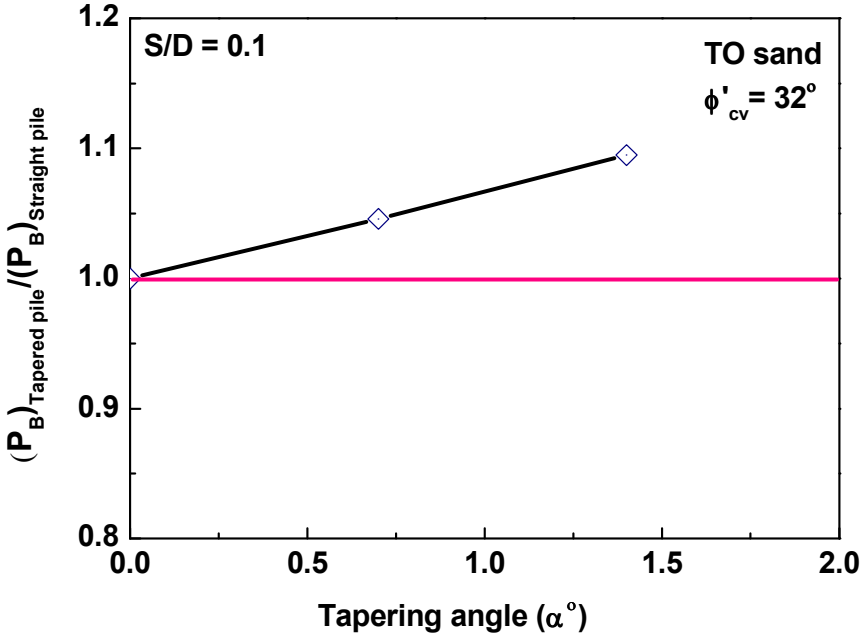

Fig. 11 Normalized end bearing capacity of TO sand at different pile tapering angle.

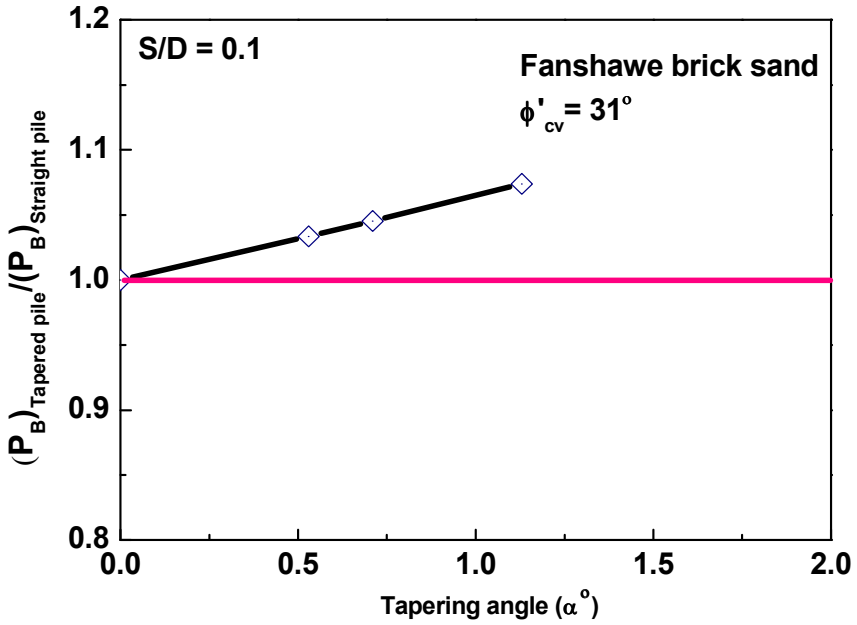

Fig. 12 Normalized end bearing capacity of Fanshawe brick sand and different pile tapering angle.

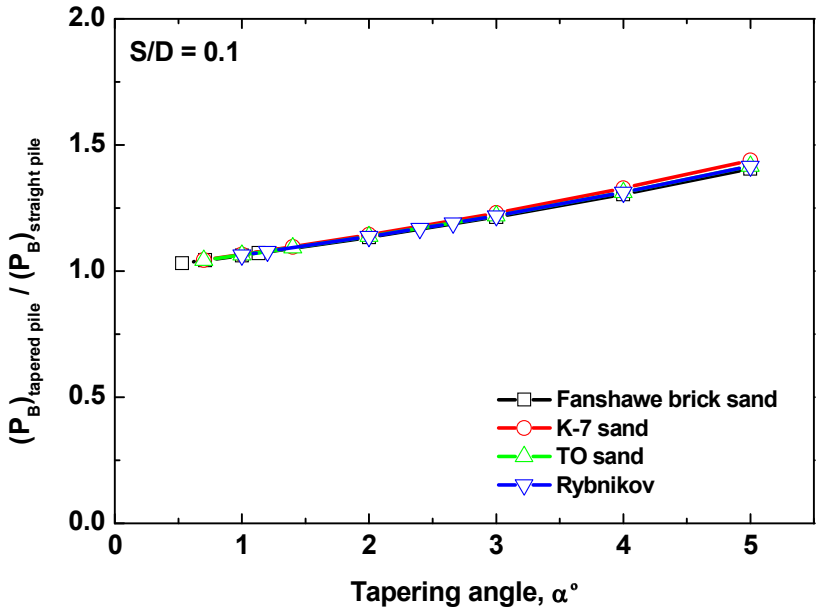

Fig. 13 Effect of tapering angle on normalized end bearing capacity at 0.1 settlement ratio.

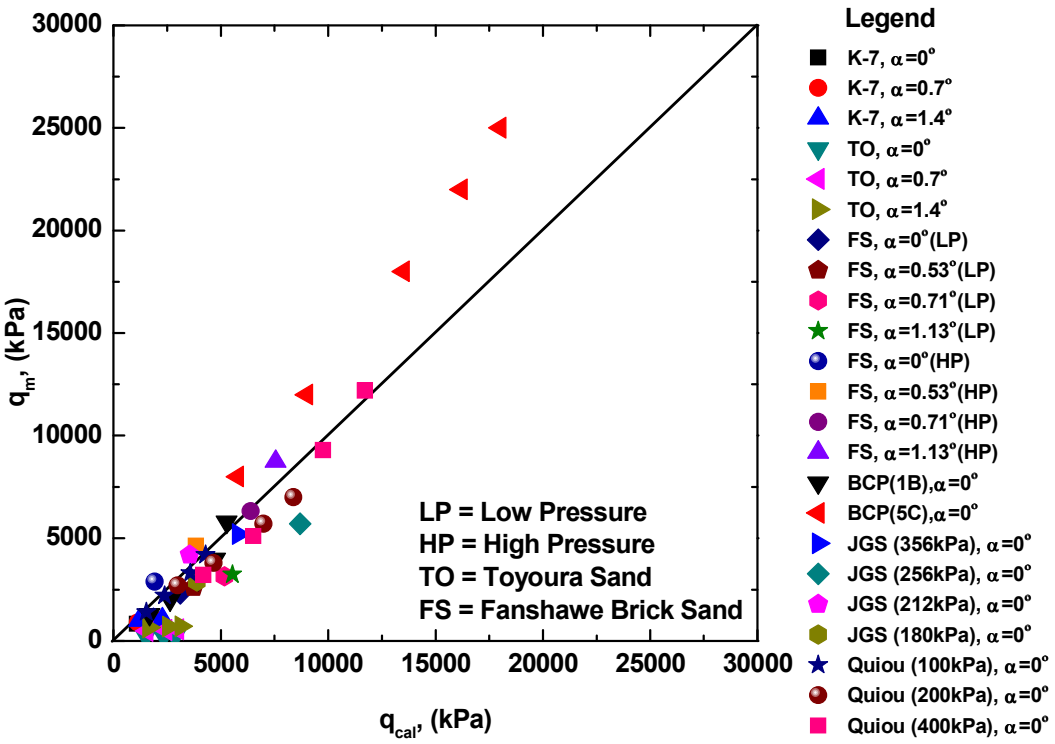

Fig. 14 Calculated and measured end bearing capacity of different types of piles.

Table 3 Pile geometry and soil characteristics from different source papers.

Source paper	No.	Pile Geometry		Soil characteristics			
		Diameter, d (m)	Length, L (m)	Soil type	σ'_v (kPa)	$\phi'_{cv,av}$ (°)	N_{av} (G) (MPa)
BCP (1B) (1971)[28]	1	0.2	4	Fine sand	60	35 (34-36)	20 (60.5)
BCP (5C) (1971)[28]	2	0.2	11	Dense sand	170	37 (36-38)	48 (133.5)
JGS data (1993)[29]	3	1.5	44.5	Sand	300	35	25 (71.1)
	4	1.5	32	Sand	356	(34-36)	30 (81)
	5	1.5	26.5	Sand	256	35	30 (81)
	6	1.5	22.4	Sand	212	(34-36)	30 (81)
Yasufuku et al. (2001)[6]	7	0.03	-	Quiou sand	100	36	- (21.9)
	8				200		- (42)
	9				400		- (47.0)

Table 4 Data arrangement for prediction and validation of end bearing capacity.

Source Paper	Soil Type	*S/D*	$\alpha = 0^o$			$\alpha = 0.53^o$			$\alpha = 0.7^o$			$\alpha = 0.71^o$			$\alpha = 1.13^o$			$\alpha = 1.4^o$		
			q_m (kPa)	q_{cal} (kPa)	q_m/q_{cal}	q_m (kPa)	q_{cal} (kPa)	q_m/q_{cal}	q_m (kPa)	q_{cal} (kPa)	q_m/q_{cal}	q_m (kPa)	q_{cal} (kPa)	q_m/q_{cal}	q_m (kPa)	q_{cal} (kPa)	q_m/q_{cal}	q_m (kPa)	q_{cal} (kPa)	q_m/q_{cal}
Manandhar (2010) [2]	K-7	0.1	828.56	1090.44	0.760				897.73	1138.77	0.788							990.76	1194.83	0.829
		0.2	862.79	1697.04	0.508	-	-	-	944.14	1772.23	0.533	-	-	-	-	-	-	1036.79	1859.50	0.558
		0.3	879.00	2083.71	0.422				970.21	2176.04	0.446							1069.29	2283.17	0.468
	TO	0.1	234.16	1504.66	0.156				473.78	1568.55	0.302							643.52	1642.46	0.392
		0.2	239.56	2341.86	0.102	-	-	-	527.81	2441.28	0.216	-	-	-	-	-	-	686.89	2556.34	0.267
		0.3	237.76	2875.67	0.083				551.23	2997.74	0.184							706.30	3139.01	0.226
Sakr et al. [11-13]	*FS (LP)	0.1	2319.49	3105.68	0.747	2603.75	3744.82	0.695	-	-	-	3147.72	5173.84	0.608	3233.34	5539.99	0.584	-	-	-
	*FS (HP)	0.1	2885.87	1932.90	1.493	4630.36	3847.47	1.204	-	-	-	6315.58	6396.16	0.987	8748.14	7554.52	1.158	-	-	-
BCP (1B) (1971) [28]	Fine sand	0.1	1300	1695.39	0.767															
		0.2	2000	2636.72	0.759															
		0.5	3000	3954.57	0.759	-	-	-	-	-	-	-	-	-	-	-	-	-	-	-
		1	4000	4745.29	0.843															
		2	5800	5272.43	1.100															
BCP (5C) (1971) [28]	Dense sand	0.1	8000	5791.11	1.38															
		0.2	12000	9007.84	1.332															
		0.5	18000	13511.25	1.332	-	-	-	-	-	-	-	-	-	-	-	-	-	-	-
		1	22000	16213.3	1.357															
		2	25000	18014.67	1.388															
JGS (1993) [29]	Sand (356 kPa)	0.13	5200	5808.52	0.895	-	-	-	-	-	-	-	-	-	-	-	-	-	-	-
	Sand (256 kPa)	0.3	5700	8691.14	0.656	-	-	-	-	-	-	-	-	-	-	-	-	-	-	-
	Sand (212 kPa)	0.08	4200	3556.08	1.181	-	-	-	-	-	-	-	-	-	-	-	-	-	-	-
	Sand (180 kPa)	0.1	2900	3895.01	0.745	-	-	-	-	-	-	-	-	-	-	-	-	-	-	-
Yasufuku et al. (2001) [6]	Quiou sand (100 kPa)	0.1	1400	1537.20	0.911															
		0.2	2200	2390.65	0.920															
		0.5	3300	3585.46	0.920	-	-	-	-	-	-	-	-	-	-	-	-	-	-	-
		1.0	4200	4302.37	0.976															
	Quiou sand (200 kPa)	0.1	2700	2997.39	0.901															
		0.2	3800	4662.05	0.815															
		0.5	5700	6992.57	0.815	-	-	-	-	-	-	-	-	-	-	-	-	-	-	-
		1.0	7000	8390.89	0.834															
	Quiou sand (400 kPa)	0.1	3200	4188.25	0.764															
		0.2	5100	6514.51	0.783															
		0.5	9300	9771.26	0.952	-	-	-	-	-	-	-	-	-	-	-	-	-	-	-
		1.0	12200	11725.31	1.041															

Note: *FS: Fanshawe brick Sand

5. Conclusion

The analytical spherical cavity expansion theory has been proposed to estimate the end bearing capacity of tapered piles. The tapering angle of the pile has been asserted to compute the end bearing capacity in the proposed model after carefully observed the benefits of tapered piles through evidences of small model tests and mobilized mechanism of the piles in the laboratory. The proposed models have been verified with results of model tests, proto type tests and real type pile tests. The main conclusions drawn from the mechanism as well as proposed models are summarized as follows:

1. The mobilized mechanism has indicated that the effective length of failure tip increases linearly with increasing tapering angle with compared to conventional straight cylindrical pile.
2. Effects of tapering angle for the parametric study show that the proposed model supports the general behavior of tapered piles to evaluate the end bearing.
3. The results have shown that about 7 % increase of the total end bearing capacity in most tapered pile at 0.1 settlement ratio. This is because the total end bearing capacity of tapered pile confines to restrain the failure mode and increase the end bearing resistance.
4. The end bearing capacity of measured and calculated results of model tests, proto type tests and real type pile tests appending various other sources have been well predicted and validated as the ideal for the evaluation of end bearing capacity of tapered piles using spherical cavity expansion theory.

6. Acknowledgement

The authors are indebted to Professor Hemant Hazarika and Associate Professor Kiyoshi Omine for their astonishing advice. In addition, heartly thanks to Laboratory Assistant Er Michio Nakashima for incessant shore up in experiments in the laboratory and colleague Mr Tohio Ishimoto, for his assistance during research.

7. References

1) S. Manandhar, N. Yasufuku, et al., Response of tapered piles in cohesionless soil based on model tests, Journal of Nepal Geological Society, Vol. 40, pp. 85-92, (2010).
2) S. Manandhar, Bearing capacity of tapered piles in sands, PhD Thesis, Kyushu University (2010).
3) A.S Vesic`, Expansions of Cavities in Infinite Soil Mass, J. Soil Mech. Fdn. Engng Am. Soc. Civ. Engrs, Vol. 98, No. SM3, pp. 265-290, (1972).
4) M.M. Baligh, Cavity Expansion in Sands with Curved Envelopes, J. Geotech. Engng Div. Am. Soc. Civ. Engrs, Vol. 102, GT11, pp. 1131-1145, (1976).
5) J.M.O. Hughes, C.P. Wroth, et al., Pressuremeter Tests in Sands, Geotechnique, London, U.K., Vol. 27, No. 4, pp. 455-477, (1977).
6) N. Yasufuku, and A.F.L. Hyde, Pile End-Bearing Capacity in Crushable Sands, Geotechnique, London, U.K., Vol. 45, No. 4, pp.663-676, (1995).
7) N. Yasufuku, H. Ochiai, and S. Ohno, Pile End-Bearing Capacity of Sand related to Soil Compressibility, Soils and Foundations, Vol. 41, No. 4, pp.59-71, (2001).
8) A. Kézdi, Pile Foundation, Foundation Engineering Handbook. 1st Ed., Ed. H. F. Winterkorn and H. Y. Fang. Van Nostrand Reinhold, New York, N.Y., pp.550-600, (1975).
9) Japanese Industrial System A 1224, Japanese Geotechnical Engineering Society, 0161, The methods and description of soil tests, First revised version, pp.59-64.

10) S. Miura, and S. Toki, A Sample Preparation Method and its Effect on Static and Cyclic Deformation-strength Properties of sand, Soils and Foundations, Japanese Geotechnical Society, Vol. 22, No.1, pp.62-77, (1982).
11) M.Sakr, M.H. El Naggar, et al., Load Transfer of Fibre-reinforced Polymer (FRP) Composite Tapered Piles in Dense Sand, Canadian Geotechnical Journal, Vol. 41, No. 1, pp.313-325, (2004).
12) M.Sakr, M.H. El Naggar, et al., Uplift Performance of FRP Tapered Piles in Dense Sand. IJPMG-Int. Jour. of Physical Modelling in Geotechnics, Vol. 2, pp.1-16, (2005).
13) M.Sakr, M.H. El Naggar, et al., Wave Equation Analyses of Tapered FRP-concrete Piles in Dense Sand, Soil Dynamics and Earthquake Engineering, Vol. 27, pp.166-182, (2007).
14) H. Ochiai, The Coefficient of Earth Pressure at Rest of Sands, Domestic Edition of Soils and Foundations, Vol. 16, No. 2, pp.105-111 (In Japanese), (1976).
15) N. Yasufuku, H. Ochiai, et al., Geotechnical Analysis of Skin Friction of Cast-in-place Piles, Proc. of 14th Int. Conf. on SMFE, Hamburg, pp.921-924, (1997).
16) N. Yasufuku, H. Ochiai, et al., Effectiveness of Critical State Friction Angle of Volcanic Ash Soils in Design Applications, Proc. of Int. Symp. on Problematic soils, IS-Tohoku, Sendai, Vol. 1, pp.189-193, (1998).
17) N. Yasufuku, H. Ochiai, et al., Geotechnical Analysis of Skin Friction of Cast-in-place Piles Related to Critical State Friction Angle, J. Geo. Engng JSCE, 617/III-46, pp.89-100 (in Japanese), (1999).
18) M.D. Bolton, What are Partial Factor for? Proc. Int. Symp. on Limit State Design in Geotecnical Engigeering, Copenhagen, Danish Geotechnical society for ISSMFE TC23, in DGF Bulletin, Vol. 10, No. 3, pp.565-583, (1993).
19) N. Miura, and Yamanouchi, Effect of Particle-crushing on the Shear Characteristics of Sand, Proc. JSCE, (260), pp.109-118 (in Japanese), (1977).
20) N. Miura, Point Resistance of Piles in Sand, Proc. 11th Int. Conf. Soil Mech., San Franscisco, Vol. 3, pp.2448-2455, (1985).
21) H. Yamaguchi, Pile End-bearing Capacity Based on an Elasto-plastic Analysis and its Application, Tsuchi-to-kiso JGS Ser. No. 209, Vol. 23, No. 7, pp.7-11 (in Japanese), (1975).
22) M. Cubrinosvski, and K. Ishihara, Empirical Correlation between SPT N-value and Relative Density for Sandy Soils, Soils and Foundations, Vol. 39, No. 5, pp.61-71, (1999).
23) H. Kishida, and A. Takano, Distribution of Contact Pressure under Base of Bored Piles in Sand, Part 1. Trans. of A.I.J., Vol. 260, pp.21-33 (in Japanese), (1977A).
24) H. Kishida, and A. Takano, Distribution of Contact Pressure under Base of Bored Piles in Sand, Part 2. Trans. of A.I.J., Vol. 260, pp.21-33 (in Japanese), (1977B).
25) H. Hirayama, Load-settlement Analysis for Bored Piles Using Hyperbolic Transfer Functions, Soils and Foundations, (1990).
26) M.H. El Naggar, M. Sakr, et al., Load Transfer of Fibre-reinforced polymer (FRP) Composite Tapered Piles in Dense sand, Canadian Geotechnical Journal, Vol. 41, No. 1, pp.313-325, (2004).
27) A.M. Rybnikov, Experimental Investigation of Bearing Capacity of Bored-cast-in-place Tapered Piles, Soil Mech. And Found. Engrg., Vol. 27, No. 2, pp.48-52, (1990).
28) BCP Committee, Field Tests on Piles in Sand, Soils and Foundations, Vol. 11, No. 2, pp.29-50, (1971).
29) Japan Geotechnical Society, JGS Standard for Vertical Load Tests of Piles, JGS, pp.151-206, (In Japanese), (1993).

Appendix I: Derivational procedure of proposed model: Ultimate end bearing capacity of tapered pile

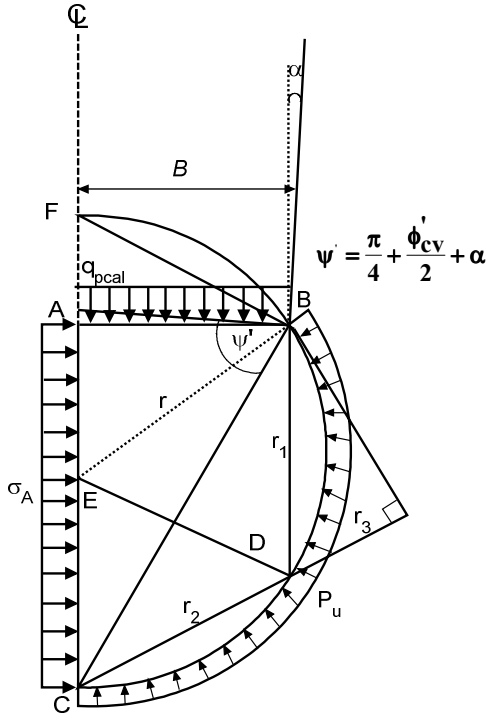

Fig. A1 - 1 Geometry of calculation procedure to find ultimate end bearing capacity of tapered pile

$$q_{pcal}\frac{B^2}{2} + \sigma_A\frac{B^2}{2}tan^2\psi' = p_u\left(\frac{r_1^2}{2} + \frac{r_2^2}{2} + r_2r_3\right) \quad \text{(A-1)}$$

$$\psi = \frac{\pi}{4} + \frac{\phi'_{cv}}{2} + \alpha \quad \text{(A-2)}$$

$$\sigma_A = q_{pcal}\frac{1-sin(\phi'_{cv}+2\alpha)}{1+sin(\phi'_{cv}+2\alpha)} \quad \text{(A-3)}$$

From **Fig. A1-1**, $r_1 = B\ tan\psi' - B\ tan\left(\frac{\pi}{4} - \frac{\phi'_{cv}}{2}\right)$

And, $r = \frac{B}{cos(\phi'_{cv}+2\alpha)}$; $AC = B\ tan\ \psi'$ such that:

$$\begin{aligned} r_1 &= AC - AF \\ &= B\ tan\ \psi' - B\ tan\ (90 - \psi') \\ &= B\ tan\left(\frac{\pi}{4} + \frac{\phi'_{cv}}{2} + \alpha\right) - B\ tan\left(90 - \frac{\pi}{4} - \frac{\phi'_{cv}}{2} - \alpha\right) \\ &= B\ tan\left(\frac{\pi}{4} + \frac{\phi'_{cv}}{2} + \alpha\right) - B\ tan\left(\frac{\pi}{4} - \frac{\phi'_{cv}}{2} - \alpha\right) \\ &= B\left[tan\left(\frac{\pi}{4} + \frac{\phi'_{cv}}{2} + \alpha\right) - tan\left(\frac{\pi}{4} - \left(\frac{\phi'_{cv}}{2} + \alpha\right)\right)\right] \end{aligned}$$

$$= B\left[\frac{\tan\frac{\pi}{4}+\tan\left(\frac{\phi'_{cv}}{2}+\alpha\right)}{1-\tan\frac{\pi}{4}\tan\left(\frac{\phi'_{cv}}{2}+\alpha\right)}-\frac{\tan\frac{\pi}{4}-\tan\left(\frac{\phi'_{cv}}{2}+\alpha\right)}{1+\tan\frac{\pi}{4}\tan\left(\frac{\phi'_{cv}}{2}+\alpha\right)}\right]$$

$$= B\left[\frac{1+\tan\left(\frac{\phi'_{cv}}{2}+\alpha\right)}{1-\tan\left(\frac{\phi'_{cv}}{2}+\alpha\right)}-\frac{1-\tan\left(\frac{\phi'_{cv}}{2}+\alpha\right)}{1+\tan\left(\frac{\phi'_{cv}}{2}+\alpha\right)}\right]$$

$$= B\left[\frac{\left(1+\tan\left(\frac{\phi'_{cv}}{2}+\alpha\right)\right)^2-\left(1-\tan\left(\frac{\phi'_{cv}}{2}+\alpha\right)\right)^2}{1-\tan^2\left(\frac{\phi'_{cv}}{2}+\alpha\right)}\right]$$

$$= B\left[\frac{1+2\tan\left(\frac{\phi'_{cv}}{2}+\alpha\right)+\tan^2\left(\frac{\phi'_{cv}}{2}+\alpha\right)-1+2\tan\left(\frac{\phi'_{cv}}{2}+\alpha\right)-\tan^2\left(\frac{\phi'_{cv}}{2}+\alpha\right)}{1-\tan^2\left(\frac{\phi'_{cv}}{2}+\alpha\right)}\right]$$

$$= B\left[\frac{4\tan\left(\frac{\phi'_{cv}}{2}+\alpha\right)}{1-\tan^2\left(\frac{\phi'_{cv}}{2}+\alpha\right)}\right]$$

$$= 2B\left[\frac{2\tan\left(\frac{\phi'_{cv}}{2}+\alpha\right)}{1-\tan^2\left(\frac{\phi'_{cv}}{2}+\alpha\right)}\right]$$

$$= 2B\tan 2\left(\frac{\phi'_{cv}}{2}+\alpha\right)$$

$$r_1 = 2B\tan\left(\phi'_{cv}+2\alpha\right) \quad \text{(A-4)}$$

$$r_2 = 2r\sin(90-\psi')$$

$$= 2r\sin\left(90-\frac{\pi}{4}-\frac{\phi'_{cv}}{2}-\alpha\right)$$

$$= 2r\sin\left(\frac{\pi}{4}-\frac{\phi'_{cv}}{2}-\alpha\right)$$

$$= \frac{2B}{\cos\left(\phi'_{cv}+2\alpha\right)}\sin\left(\frac{\pi}{4}-\frac{\phi'_{cv}}{2}-\alpha\right) \quad \text{(A-5)}$$

$$r_3 = r_1\cos\psi'$$

$$= 2B\tan\left(\phi'_{cv}+2\alpha\right)\cos\left(\frac{\pi}{4}+\frac{\phi'_{cv}}{2}+\alpha\right) \quad \text{(A-6)}$$

Substituting Equations (A-2) to (A-6) for ψ', σ_A, r_1, r_2, and r_3 into Equation (A-1), the Left Hand and Right Hand parameters become Equations (A-7) and (A-8) respectively.

$$\text{L. H. S.} = q_{pcal}\frac{B^2}{2}+\sigma_A\frac{B^2}{2}\tan^2\psi'$$

$$= \frac{B^2}{2}q_{pcal}+\left[\frac{B^2}{2}\frac{1-\sin\left(\phi'_{cv}+2\alpha\right)}{1+\sin\left(\phi'_{cv}+2\alpha\right)}\tan^2\psi'\right]$$

$$= \frac{B^2}{2}q_{pcal}\left[\frac{1-\sin\left(\phi'_{cv}+2\alpha\right)}{1+\sin\left(\phi'_{cv}+2\alpha\right)}\frac{1+\sin\left(\phi'_{cv}+2\alpha\right)}{1-\sin\left(\phi'_{cv}+2\alpha\right)}+1\right]$$

$$= \frac{B^2}{2} q_{pcal}[2]$$
$$= B^2 q_{pcal} \quad \text{(A-7)}$$

$$\text{R. H. S} = p_u \left(\frac{r_1^2}{2} + \frac{r_2^2}{2} + r_2 r_3 \right)$$

$$= p_u \left[\left(\frac{2B \tan\left(\phi'_{cv} + 2\alpha\right)}{2} \right)^2 + \left(\frac{\frac{2B}{\cos\left(\phi'_{cv} + 2\alpha\right)} \sin\left(\frac{\pi}{4} - \frac{\phi'_{cv}}{2} - \alpha \right)}{2} \right)^2 \right.$$
$$\left. + \frac{2B}{\cos\left(\phi'_{cv} + 2\alpha\right)} \sin\left(\frac{\pi}{4} - \frac{\phi'_{cv}}{2} - \alpha \right) . 2B \tan\left(\phi'_{cv} + 2\alpha\right) \cos\left(\frac{\pi}{4} + \frac{\phi'_{cv}}{2} + \alpha \right) \right]$$

$$= \frac{\left(2B \tan\left(\phi'_{cv} + 2\alpha\right)\right)^2}{2} p_u$$
$$+ \left[\frac{2B \sin\left(\frac{\pi}{4} - \frac{\phi'_{cv}}{2} - \alpha \right)}{\cos\left(\phi'_{cv} + 2\alpha\right)} \left(\frac{2B \sin\left(\frac{\pi}{4} - \frac{\phi'_{cv}}{2} - \alpha \right)}{2 \cos\left(\phi'_{cv} + 2\alpha\right)} \right.\right.$$
$$\left.\left. + \ 2B \tan\left(\phi'_{cv} + 2\alpha\right) \cos\left(\frac{\pi}{4} + \frac{\phi'_{cv}}{2} + \alpha \right) \right) p_u \right]$$

$$= p_u \left[2B^2 \tan\left(\phi'_{cv} + 2\alpha\right) + \frac{2B^2 \sin^2\left(\frac{\pi}{4} - \frac{\phi'_{cv}}{2} - \alpha \right)}{\cos^2\left(\phi'_{cv} + 2\alpha\right)} \right.$$
$$\left. + \frac{4B^2 \ \tan\left(\phi'_{cv} + 2\alpha\right) \sin\left(\frac{\pi}{4} - \frac{\phi'_{cv}}{2} - \alpha \right) \cos\left(\frac{\pi}{4} + \frac{\phi'_{cv}}{2} + \alpha \right)}{\cos\left(\phi'_{cv} + 2\alpha\right)} \right]$$

$$= p_u \left[2B^2 \left(\tan\left(\phi'_{cv} + 2\alpha\right) + \frac{\sin^2\left(\frac{\pi}{4} - \frac{\phi'_{cv}}{2} - \alpha \right)}{\cos^2\left(\phi'_{cv} + 2\alpha\right)} \right.\right.$$
$$\left.\left. + \frac{2B^2 \ \sin\left(\phi'_{cv} + 2\alpha\right) \sin\left(\frac{\pi}{4} - \frac{\phi'_{cv}}{2} - \alpha \right) \cos\left(\frac{\pi}{4} + \frac{\phi'_{cv}}{2} + \alpha \right)}{\cos^2\left(\phi'_{cv} + 2\alpha\right)} \right) \right]$$

$$= p_u \left[2B^2 \left(\frac{\sin^2\left(\phi'_{cv} + 2\alpha\right) \ + \ \frac{\left(1 - \sin\left(\phi'_{cv} + 2\alpha\right)\right)}{2} \ + \ \sin\left(\phi'_{cv} + 2\alpha\right) \left(1 - \sin\left(\phi'_{cv} + 2\alpha\right)\right)}{\cos^2\left(\phi'_{cv} + 2\alpha\right)} \right) \right]$$

$$= p_u 2B^2 \left[\left(\frac{sin^2(\phi'_{cv} + 2\alpha) + \frac{\left(1 - sin(\phi'_{cv} + 2\alpha)\right)}{2} + sin(\phi'_{cv} + 2\alpha)\left(1 - sin(\phi'_{cv} + 2\alpha)\right)}{\left(1 - sin(\phi'_{cv} + 2\alpha)\right)\left(1 + sin(\phi'_{cv} + 2\alpha)\right)} \right) \right]$$

$$= p_u 2B^2 \left[\left(\frac{2\,sin^2(\phi'_{cv} + 2\alpha) + \left(1 - sin(\phi'_{cv} + 2\alpha)\right) + 2\,sin(\phi'_{cv} + 2\alpha)\left(1 - sin(\phi'_{cv} + 2\alpha)\right)}{2\left(1 - sin(\phi'_{cv} + 2\alpha)\right)\left(1 + sin(\phi'_{cv} + 2\alpha)\right)} \right) \right]$$

$$= p_u B^2 \left[\left(\frac{2\,sin^2(\phi'_{cv} + 2\alpha) + \left(1 - sin(\phi'_{cv} + 2\alpha)\right) + 2\,sin(\phi'_{cv} + 2\alpha) - 2\,sin^2(\phi'_{cv} + 2\alpha)}{\left(1 - sin(\phi'_{cv} + 2\alpha)\right)\left(1 + sin(\phi'_{cv} + 2\alpha)\right)} \right) \right]$$

$$= p_u B^2 \left[\frac{1 + sin(\phi'_{cv} + 2\alpha)}{\left(1 - sin(\phi'_{cv} + 2\alpha)\right)\left(1 + sin(\phi'_{cv} + 2\alpha)\right)} \right]$$

$$= \frac{B^2}{\left(1 - sin(\phi'_{cv} + 2\alpha)\right)} p_u \qquad \text{(A-8)}$$

Comparing Equations (A-6) and (A-7) gives,

$$B^2 q_{pcal} = \frac{B^2}{\left(1 - sin(\phi'_{cv} + 2\alpha)\right)} p_u$$

Thus,

$$q_{pcal} = \frac{1}{\left(1 - sin(\phi'_{cv} + 2\alpha)\right)} p_u \qquad \text{(A-9)}$$